THE JOURNAL OF PHYSICAL CHEMISTRY C

Article

pubs.acs.org/JPCC

Adsorption of Metallic, Metalloidic, and Nonmetallic Adatoms on Two-Dimensional C_3N

Meysam Makaremi,[†] Bohayra Mortazavi,[‡] and Chandra Veer Singh*[,†,§]

[†]Department of Materials Science and Engineering, University of Toronto, 184 College Street, Suite 140, Toronto, Ontario M5S 3E4, Canada

[‡]Institute of Structural Mechanics, Bauhaus-Universität Weimar, Marienstr. 15, D-99423 Weimar, Germany

[§]Department of Mechanical and Industrial Engineering, University of Toronto, 5 King's College Road, Toronto, Ontario M5S 3G8, Canada

Supporting Information

ABSTRACT: Two-dimensional polyaniline with a C_3N stoichiometry is a newly fabricated material that is expected to possess fascinating electronic, thermal, mechanical, and chemical properties. The possibility of further tuning the C_3N properties upon the adsorption of foreign adatoms is thus among the most attractive research. We carried out extensive ab initio density functional theory simulations to investigate the adsorption of various elements including nonmetallic, metalloidic, and metallic elements on the C_3N monolayer. While pristine C_3N acts as a semiconductor with an indirect electronic band gap; the functionalization with nonmetallic and semimetallic elements leads to a p-type doping and induces metallic behavior to the monolayer. On the contrary, metallic adsorption depending on the adatom size and the number of valence electrons may result in semiconducting, half-metallic, or metallic properties. Whenever metallic foreign atoms conduct metallic characteristics, they mostly lead to the n-type doping by electron donation to the surface. Moreover, adsorption of transition metals could enhance the magnetic behavior of the monolayer due to the contribution of d electronic states. These results suggest that C_3N illustrates viable electromagnetic properties that could be promising for semiconducting, nanosensor, and catalytic applications.

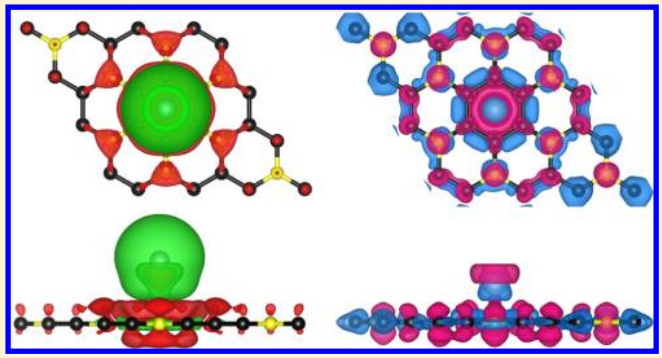

1. INTRODUCTION

A new class of materials called 2D crystals has attracted extensive attention since the extraction and characterization of graphene from bulk graphite under controlled conditions in the past decade.[1] These single atomic layer crystals provide exceptional chemical, physical, and mechanical characteristics quite distinctive from their original 3D bulk crystals.[2−5] During the past decade, most of 2D monolayer structures such as graphene, hexagonal boron-nitride (h-BN), and MoS_2 have been extracted from layered bulk materials composed of weakly van-der-Waals-bound stacked layers. Because the number of these layered materials is limited, the extracted 2D crystals are restricted to a handful of species. To resolve this issue, a new generation of these materials called synthetic 2D crystals has been recently grown and fabricated. The fabrication process does not require the initial bulk counterparts, and one can gain complementary functionalities and characteristics through designing and tuning the fabrication method.[6,7] In recent years, several honeycomb monolayers from group IV of elements, such as silicene, germanene, and stanene, have been synthesized and grown on different substrates.[8−12]

Several approaches have been developed to modify the electromagnetic properties of 2D monolayers after the fabrication. These methods involve substitutional doping, defect engineering, functionalizing with adatoms, and applying electric field and strain, among which surface functionalization can be considered as a robust approach.[13−18] Several computational studies have been conducted to investigate adatom adsorption on 2D monolayers. In one of the first studies in this field, Chan et al. investigated the adsorption of foreign elements on graphene by using density functional theory (DFT) simulations.[19] The functionalization of silicene by metallic adatoms was studied, and it found that as a consequence of the buckled structure and the different surface reactivity the interaction of silicene with adatoms is not comparable to that of graphene.[20] Adsorption properties of germanene, stanene, tin sulfide, and graphene derivatives interacting with different foreign atoms consisting of alkali, alkaline-earth, transition metallic elements, and non-metallic elements were the subjects of next investigations.[21−25]

Most recently, 2D polyaniline (C_3N) has been synthesized by the direct pyrolysis of hexaaminobenzene (HAB) trihydrochloride single crystals, and it has been characterized by scanning

Received: May 10, 2017
Revised: August 1, 2017
Published: August 1, 2017

ACS Publications © 2017 American Chemical Society

DOI: 10.1021/acs.jpcc.7b04511
J. Phys. Chem. C 2017, 121, 18575−18583

tunneling microscopy and scanning tunneling spectroscopy.[26] This novel material is predicted to offer good performance in a variety of applications, such as solution−membrane interfaces,[27] solar cell devices,[28] and electrolyte gating and doping of transistors,[29] as a consequence of the stoichiometric formula of C_3N and graphene-like structure in which nitrogen uniformly is distributed.[30,31] Recent theoretical studies confirmed that C_3N can yield ultrahigh stiffness and thermal conductivity.[32,33] As can be seen in Figure 1, the C_3N honeycomb structure consists of two types of hexagonal rings including the CC rings with six carbon atoms and the NC rings with two nitrogen and four carbon atoms. The C−C and C−N bonds both involve a similar atomic bond length of 1.40 Å. C_3N involves a monoclinic unit cell with lattice constants $a = b = 4.8614$ Å containing eight atoms (6 C and 2 N atoms). Functionalization of C_3N monolayer by foreign atoms is expected to result in fascinating properties for this new 2D crystal but has not been studied so far.

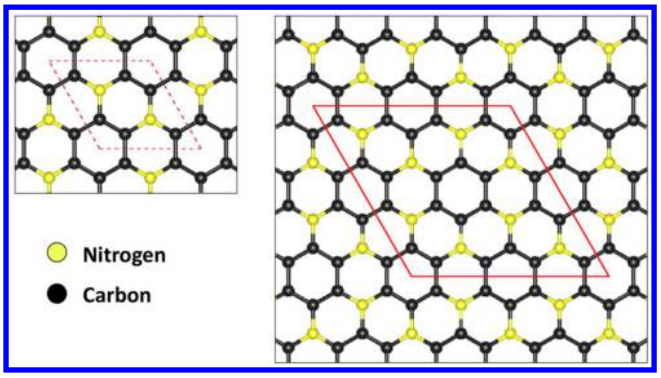

Figure 1. C_3N unit cell (dashed red line) and 2 × 2 supercell (solid red line).

In the present work, we performed first-principles electronic structure calculations to probe the role of various functionalizing elements consisting of metallic adatoms, such as alkali (AM), alkaline earth (AEM), Al and 3d transition metallic (TM) elements, and semimetallic/nonmetallic adatom such as H, B, C, N, O, F, and P on electromagnetic characteristics of C_3N. Properties including the binding energy, total density of electronic states (TDOS), partial density of electronic states (PDOS), Bader charge transfer, and the total magnetization were investigated in detail for each adatom. We first calculated the electronic structure properties of the bare monolayer. Next, the adsorption of metalloids and nonmetals on the monolayer was considered; finally, we studied the electromagnetic properties of the C_3N surface functionalized by various metallic species and compared with those of the former species.

2. COMPUTATIONAL DETAILS

Using the Vienna Ab-initio Simulation Package (VASP),[34] we carried out first-principles simulations based on spin-polarized DFT to study the interaction of the C_3N monolayer with various adsorbing foreign atoms. Projector augmented wave (PAW) potentials[35] and generalized gradient approximation (GGA) with the Perdew−Burke−Ernzerhof (PBE) functionals[36] were used to describe pseudopotential and exchange correlation functional terms, respectively. For alkali atoms Na and K, we considered p semicore states as valence states by choosing the Na_pv and K_pv pseudopotentials, respectively. The van der Waals DFT-D2[37] correction method of Grimme was applied to modify binding energy calculations. In addition to PBE simulations, Heyd−Scuseria−Ernzerhof (HSE06)[38] functionals were used to calculate the density of states for some cases. The Brillouin zone integration was performed through the Monkhorst−Pack scheme[39] with a mesh grid of 15 × 15 × 1. A kinetic energy cutoff of 500 eV and an electron self-consistent convergence criterion of 1×10^{-6} eV were considered for calculations. For ionic relaxation the conjugate gradient method is applied with the force convergence criterion of 1×10^{-3} eV/Å to minimize the Hellmann−Feynman forces. The tetrahedron method with Blöchl corrections was used as the smearing scheme.

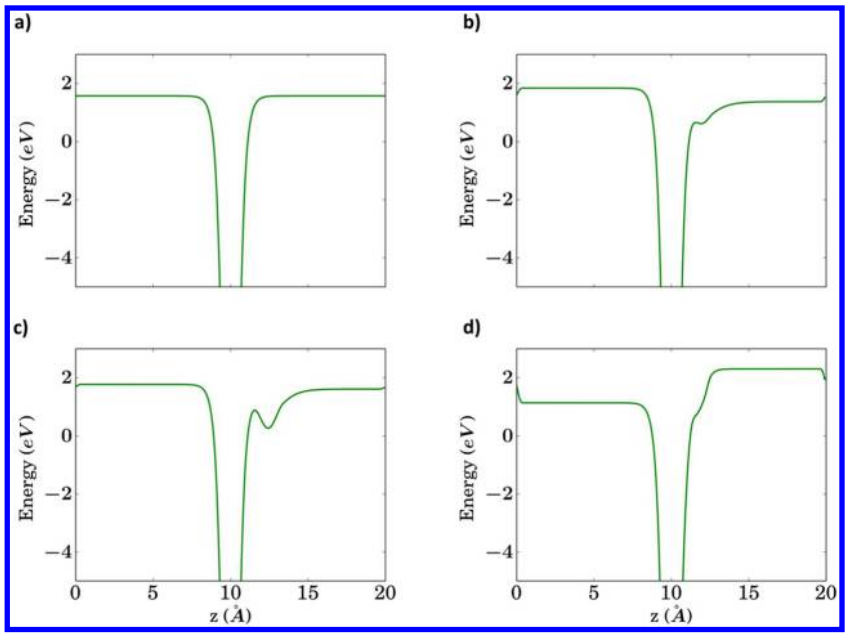

Figure 2. Average planar potential in the z direction for pristine C_3N (a) and the C_3N monolayer interacting with Li (b), Na (c), and O (d). The work function (Φ) can be calculated from $\Phi = E_{vac} - \epsilon_F$, in which E_{vac} and ϵ_F are the vacuum potential and Fermi level energy, respectively. From this formula, we predicted the work-function of the bare monolayer and functionalized monolayers with Li, Na, and O to be 3.11, 2.73, 2.76, and 3.21 respectively.

DOI: 10.1021/acs.jpcc.7b04511
J. Phys. Chem. C 2017, 121, 18575−18583

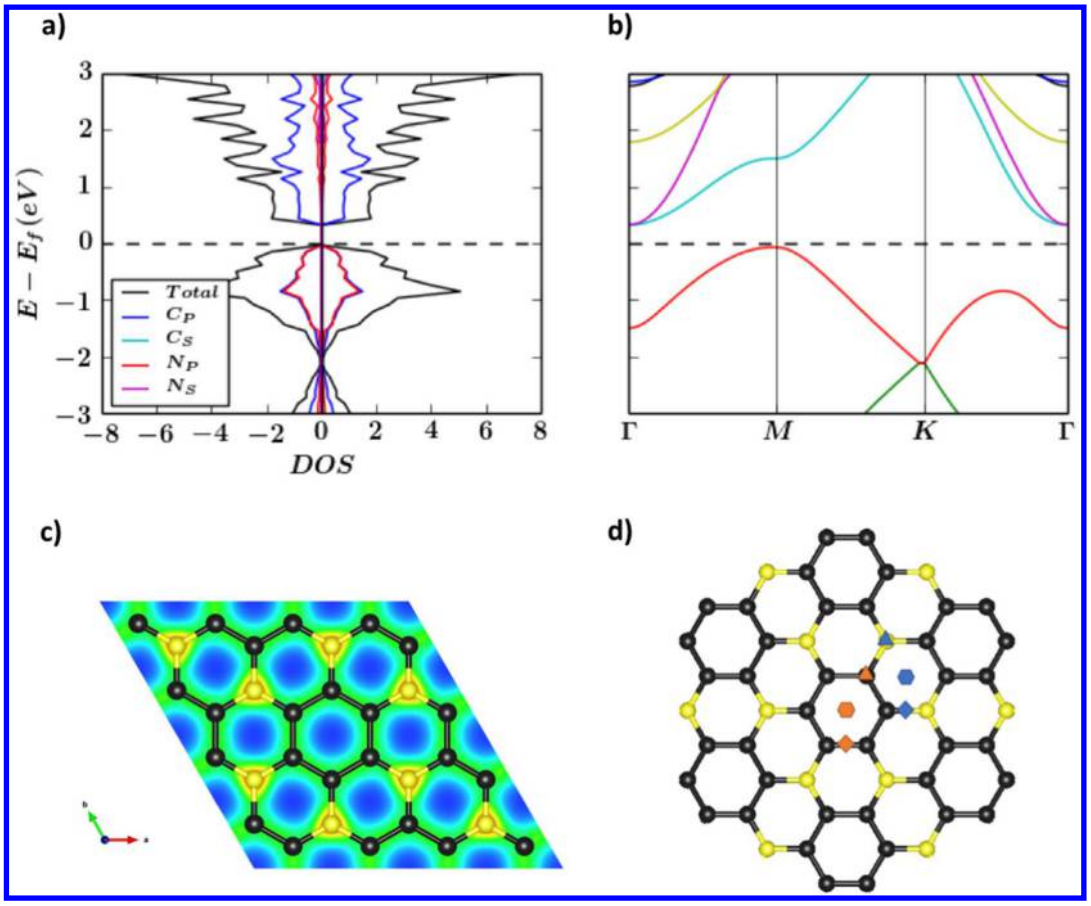

Figure 3. Electronic structure properties of C_3N. (a) Spin-polarized projected density of states. The black dashed line shows the Fermi energy level. (b) Electronic band structure. (c) Electronic charge distribution. (d) Considered adsorption sites on the C_3N surface, illustrated by orange and blue diamonds for C−C and N−C bridge sites (B_{CC} and B_{NC}); orange and blue hexagons for C−C and C−N hexagonal sites (H_{CC} and H_{NC}); and orange and blue triangles for C and N tetrahedral sites (T_C and T_N), respectively.

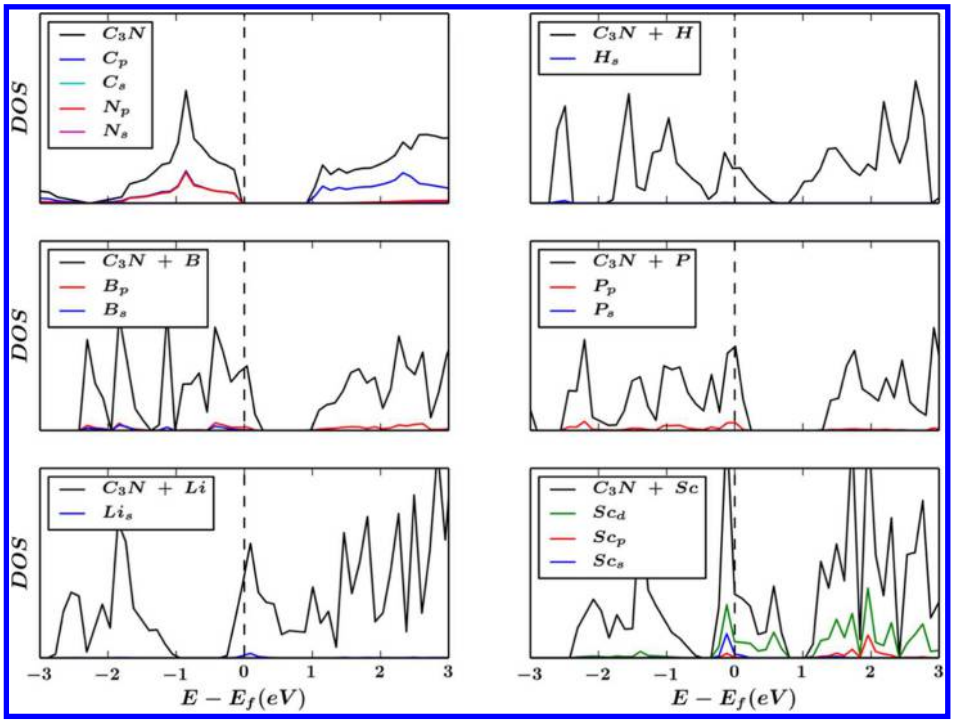

Figure 4. HSE06 density of states for the pristine monolayer and the monolayer functionalized by H, B, P, Li, and Sc adatoms.

DOI: 10.1021/acs.jpcc.7b04511
J. Phys. Chem. C 2017, 121, 18575−18583

Table 1. Electromagnetic Properties of 2D C_3N Interacting with Non/Semimetallic Adatoms[a]

	C_3N						graphene[b]		
element	$site_{Ads}$	E_{Ads} (eV)	D_{Ads} (Å)	E_g (eV)	$\Delta\rho$ (e)	μ [μ_β]	$site_{Ads}$	E_{Ads} (eV)	$\Delta\rho$ (e)
H	T_C	−1.64	1.12	M	−0.04	0	T_C	−1.96	−0.15
B	B_{CC}	−1.57	1.64	M	−1.59	0	B_{CC}	−1.77	−0.43
C	B_{CC}	−2.86	1.52	M	+0.15	0	B_{CC}	−3.34	+0.02
N	B_{CC}	−2.63	1.43	M	+1.83	0	B_{CC}	−4.56	+0.68
O	T_C	−3.64	1.30	M	+1.79	0	B_{CC}	−4.79	+0.84
F	T_C	−2.89	1.59	M	+0.59	0	T_C	−2.90	+0.59
P	B_{CC}	−1.26	1.88	M	−1.87	0	B_{CC}	−2.20	−0.38

[a]$Site_{Ads}$, E_{Ads}, D_{Ads}, E_g, $\Delta\rho$, and μ show the adsorption site, the binding energy, the bond length between the adatom and the closest surface atom, the band gap, the Bader charge transfer from the adatom to C_3N, and the total magnetic moment, respectively. [b]Graphene data calculated by ref 42.

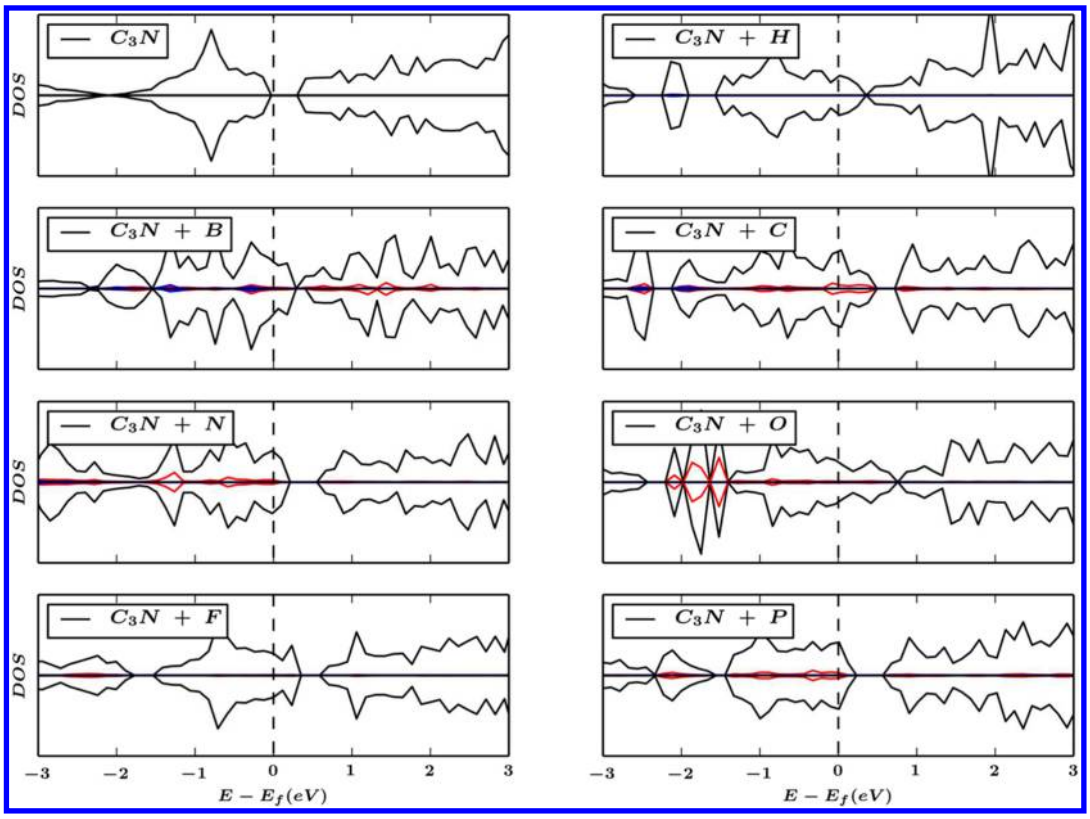

Figure 5. Density of states for the pristine and the functionalized C_3N monolayer interacting with non/semimetallic elements. The black line shows TDOS, and colorful lines illustrate the PDOS of functionalizing adatoms. Solid blue and red lines represent s and p states, respectively.

As shown in Figure 1, a 2 × 2 supercell including 24 carbon and 8 nitrogen atoms was used for all simulations, and a vacuum space of 20 Å was applied in the sheet normal direction. To find the optimal size for the vacuum space, the convergence test with respect to the box dimension in the z direction was performed (see Figure S1), and the effect of adatom adsorption on the work function was probed for three different elements including P, Li, and Na by calculating the Fermi level energy and the average planar energy in the z direction (see Figure 2). The grid-based Bader scheme[40] was used to analyze the charge distribution, and charge difference resulting from the functionalization is explained as

$$\Delta\rho_{Ads} = \rho_{C_3N+Atom} - \rho_{C_3N} - \rho_{Atom} \quad (1)$$

Here $\rho_{C_3N+Atom}$, ρ_{C_3N}, and ρ_{Atom} are the total charges of the C_3N/adatom system, the pristine monolayer, and the isolated adatom, respectively. In addition, adsorption energy of the adatom on the C_3N surface is calculated by

$$E_{Ads} = E_{C_3N+Atom} - E_{C_3N} - E_{Atom} \quad (2)$$

where $E_{C_3N+Atom}$, E_{C_3N}, and E_{Atom} are the total energies of the C_3N/adatom system, pristine C_3N. and the isolated adatom, respectively. A large negative value of E_{Ads} signifies strong binding.

To study the effect of adatom adsorption on the magnetic characteristics of the monolayer, the magnetic ground state needs to be identified. Because this property is quite sensitive to the initial conditions, we manually searched the ground state for each system by considering various magnetic configurations including different initial magnetic moments and net magnetizations; later, we examined the consistency of the results after relaxation. Otherwise, the structure involving the minimum energy was chosen as the most possible adsorption configuration.

DOI: 10.1021/acs.jpcc.7b04511
J. Phys. Chem. C 2017, 121, 18575−18583

3. RESULTS AND DISCUSSION

To analyze the functionalization process, it is always useful to probe the electronics properties of pristine C_3N at the first step.

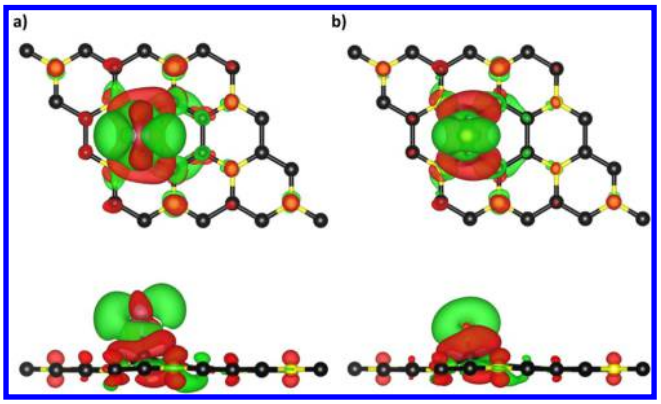

Figure 6. Differential charge density of the C_3N monolayer functionalized by non/semimetallic adatoms: (a) P and (b) N. Color coding consists of red for charge gain and green for charge loss.

Total density of states and projected density of states of the bare monolayer, illustrated in Figure 3a, reveal that the valence band maximum is composed of p orbitals of both carbon and nitrogen, whereas the conduction band minimum is mainly derived by the contribution of the p orbitals of carbon atoms. Figure 3b depicts the electronic band structure of C_3N, which suggests an indirect energy gap of E_g = 0.39 eV between the Γ point and the M point resulting in semiconducting nature of the bare monolayer. It is well known that PBE underestimates the energy gap; therefore, we performed HSE06 functional calculations suggesting that the electronic density is similar to that of PBE and only the conduction band is shifted upward, leading to an energy gap of E_g = 1.05 eV (see Figure 4). The result is consistent with the literature[34,41] and verifies the accuracy of our modeling.

To study atomic adsorption, we investigated the adsorption effect of 24 different adatoms from different atomic species. As illustrated in Figure 3d, six potential adsorption sites on the C_3N surface were considered: (1) the bridge site above the midpoint of the C−C bond (B_{CC}), (2) the bridge site above the midpoint of the N−C bond (B_{NC}), (3) the hexagonal site on the center of the ring with six C atoms (H_{CC}), (4) the hexagonal site on the center of the ring composed of both C and N atoms (H_{NC}), (5) the tetrahedral site on top of the C atom (T_C), and the tetrahedral site on top of the N atom (T_N). To further ensure that the functionalized C_3N nanomembranes were thermodynamically stable, after the relaxation step, we carried out DFT molecular dynamics simulations at 1000 K for some systems involving P, Al, C, N, Mg, Cr, Co, and Ni adatoms interacting with C_3N.

3.1. Adsorption of Non/Semimetallic Foreign Adatoms. We investigated the role of common functionalizing nonmetallic and metalloidic agents including H, B, C, N, O, F, and P on electromagnetic characteristics of C_3N. The results summarized in Table 1 indicate that the only carbon atoms of the monolayer act as binding sites, whereas no adsorption occurs on the nitrogen atoms. Among the studied nonmetallic and metalloidic agents, the most reactive one is O with a binding energy (E_{Ads}) of −3.64 eV as a consequence of its large number of valence electrons and short atomic radius; however, the shortest adsorption bond distance (D_{Ads}) belongs to H, which includes the shortest atomic radius among the studied foreign atoms. It is worth noting that the species prefer to be adsorbed at B_{CC} and T_C sites of C_3N, similar to the way they interact with the graphene surface, and also, similar to graphene, C_3N makes the strongest bonds with O, F, C, and N.

Electronic density of states calculations of functionalizing nonmetallic and metalloidic species depicted in Figure 5 suggests that the interaction of the species with the monolayer eliminates the semiconducting band gap of pristine C_3N and induces metallic properties. These adsorptions mostly produce a p-type carrier by shifting the Fermi level to the valence band edge. Listed in Table 1, the Bader analysis indicates that due to the electronegativity difference between the surface adsorbing atoms and the binding foreign atoms the adsorption of

Table 2. Electromagnetic Properties of 2D C_3N Monolayer Interacting with Metallic Adatoms[a]

	C_3N						graphene[b]		
element	$site_{Ads}$	E_{Ads} (eV)	D_{Ads} (Å)	E_g (eV)	$\Delta\rho$ (e)	μ (μ_β)	$site_{Ads}$	E_{Ads} (eV)	$\Delta\rho$ (e)
Li	H_{CC}	−0.80	2.33	M	−0.87	0.0	H_{CC}	−1.36	−0.86
Na	H_{CC}	−0.33	2.77	M	−0.71	0.0	H_{CC}	−0.72	−0.62
K	H_{CC}	−0.44	3.09	M	−0.63	0.0	H_{CC}	−0.81	−0.63
Be	H_{CC}	−0.11	3.08	0.41	−0.03	0.0	H_{CC}	−0.12	−0.05
Mg	H_{CC}	−0.09	3.32	0.40	−0.13	0.0	H_{CC}	−0.03	−0.10
Ca	H_{CC}	−0.43	2.72	M	−0.80	0.0	H_{CC}	−0.52	−0.85
Al	H_{CC}	−0.89	2.57	M	−1.25	0.0	H_{CC}	−1.62	−0.81
Sc	H_{CC}	−1.84	2.30	M	−1.24	1.1	H_{CC}	−2.08	−1.10
Ti	H_{CC}	−2.25	2.30	M	−1.05	2.8	H_{CC}	−3.27	−1.10
V	H_{CC}	−1.36	2.13	M	−1.13	1.0	H_{CC}	−3.88	−0.98
Cr	T_C	−0.25	2.03	0.23	−1.01	0.0	H_{CC}	−3.99	−0.84
Mn	H_{CC}	−0.37	2.43	HM	−0.48	5.0	H_{CC}	−3.82	−0.70
Fe	H_{CC}	−1.39	2.09	M	−0.61	2.0	H_{CC}	−3.83	−0.58
Co	H_{CC}	−1.72	2.04	M	−0.49	0.0	H_{CC}	−3.64	−0.48
Ni	H_{CC}	−1.98	2.08	0.49	−0.41	0.0	H_{CC}	−3.08	−0.45
Cu	T_C	−0.71	2.03	M	−0.08	0.1	B_{CC}	−0.97	−0.19
Zn	H_{CC}	−0.24	3.30	0.38	−0.04	0.0	H_{CC}	−0.13	−0.03

[a]$Site_{Ads}$, E_{Ads}, D_{Ads}, E_g, $\Delta\rho$, and μ show the adsorption site, the binding energy, the bond length between the adatom and the closest surface atom, the band gap, the Bader charge transfer from the adatom to C_3N, and the total magnetic moment, respectively. [b]Graphene data calculated by ref 42.

DOI: 10.1021/acs.jpcc.7b04511
J. Phys. Chem. C 2017, 121, 18575−18583

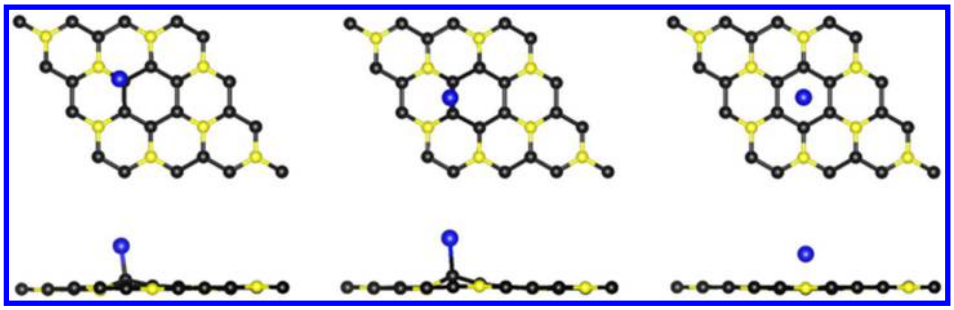

Figure 7. Adsorption configurations of the foreign adatom on C_3N. From left to right, atomic adsorption on T_C, B_{CC}, and H_{CC} sites. The blue ball represents the adatom.

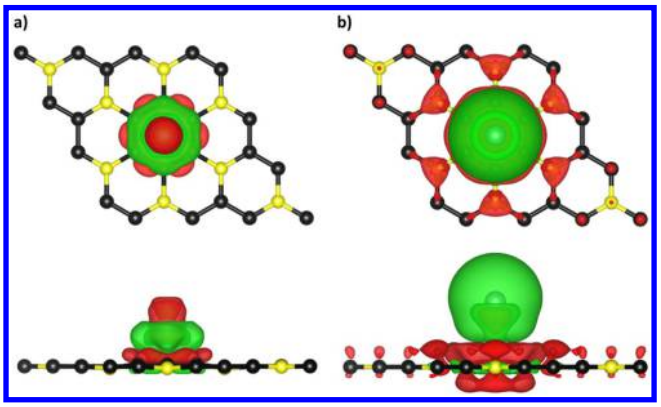

Figure 8. Differential charge density of the C_3N monolayer functionalized by metallic adatoms: (a) Ni and (b) Be. Color coding of red and green illustrates the charge gain and charge loss, respectively.

nonmetallic and metalloidic atoms may result in a spectrum of charge transfer in which the maximal charge gain belongs to the phosphorus adsorption with a charge transfer of −1.87 e, and the maximal charge loss happens due to the bonding of nitrogen including a charge induction of +1.83 e. (See Figure 6.)

3.2. Adsorption of Metallic Foreign Adatoms. We calculated the adsorption properties of 17 metallic elements including alkali (Li, Na, and K), alkaline-earth (Be, Mg, and Ca), group III (Al), and 3d transition (Sc, Ti, V, Cr, Mn, Fe, Co, Ni, Cu, and Zn) metals. As illustrated in Table 2, similar to the former species, metallic ones avoid the nitrogen atoms of C_3N. Also, metals tend to be adsorbed on H_{CC} and T_C sites while nonmetallic and metalloidic atoms prefer B_{CC} and T_C sites (see Figure 7), which is similar to the interactions with graphene. The only exception occurs for Cu, which prefers to be adsorbed on the B_{CC} site of graphene. It is worth to noting that the adsorption on B_{CC} and T_C sites results in the local distortion of the

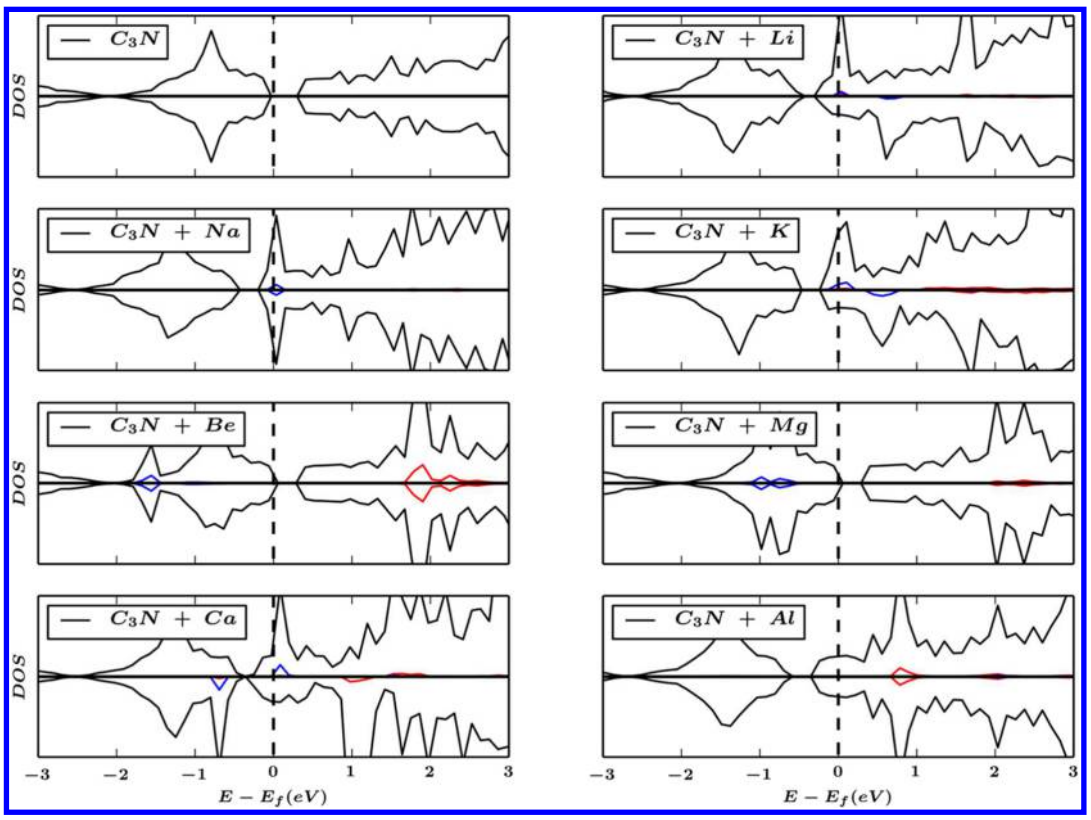

Figure 9. Density of states for the pristine and the functionalized C_3N monolayer interacting with alkali, alkali earth, and group III metallic elements. The black line shows TDOS and colorful lines illustrate the PDOS of functionalizing adatoms. Solid blue and red lines show s and p states, respectively.

DOI: 10.1021/acs.jpcc.7b04511
J. Phys. Chem. C 2017, 121, 18575−18583

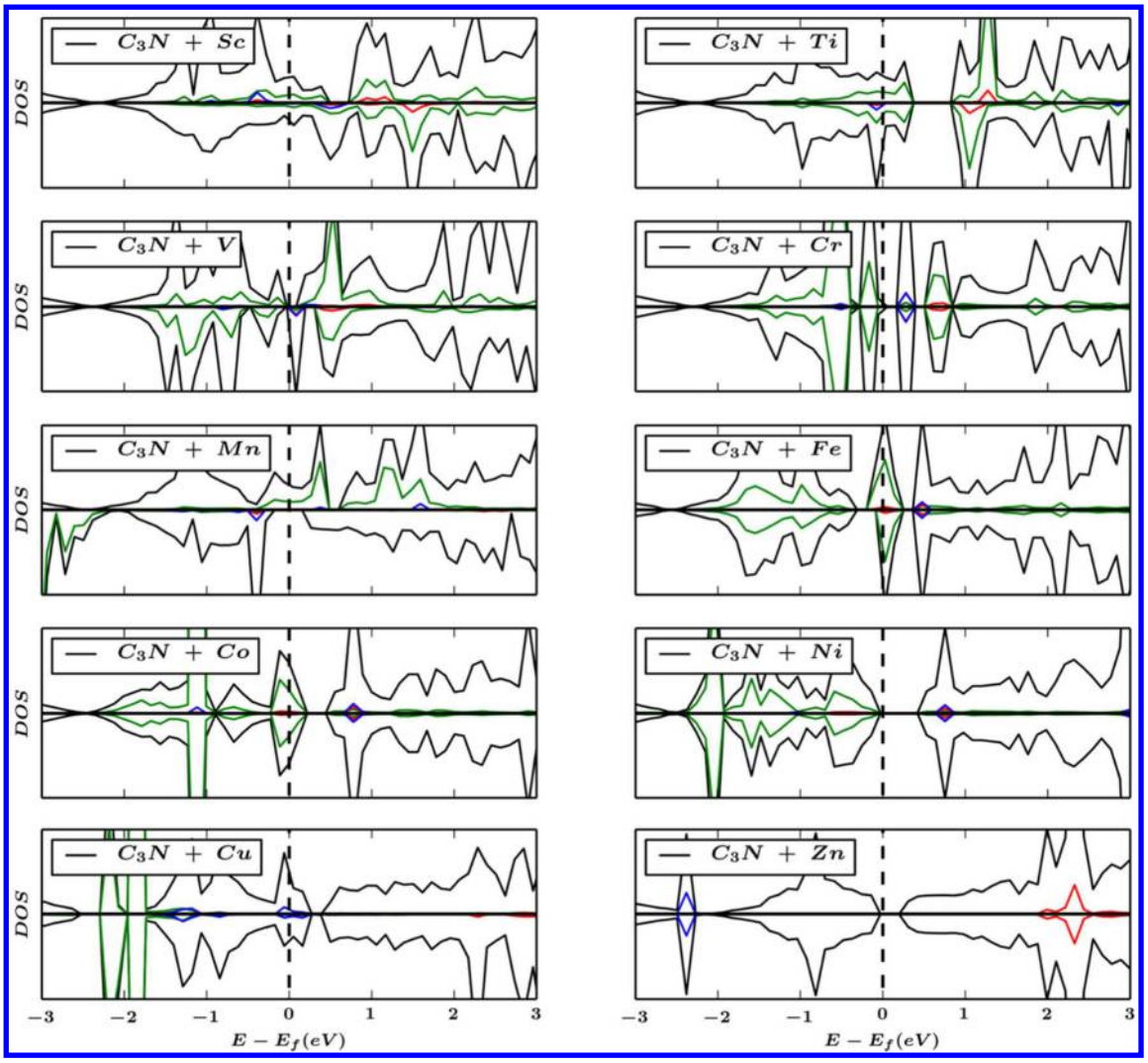

Figure 10. Density of states for the pristine and the functionalized C_3N monolayer interacting with 3d transition metallic elements. The black line represents TDOS and colorful lines illustrate the PDOS of functionalizing adatoms. Solid blue, red, and green lines shows s, p, and d states, respectively.

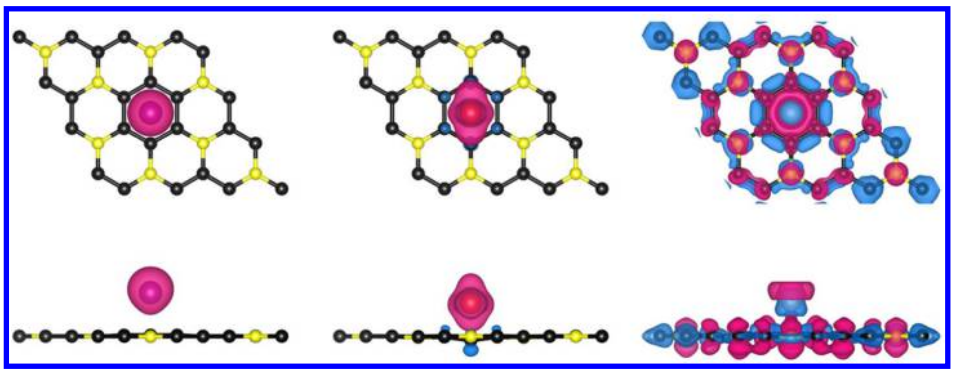

Figure 11. Different C_3N magnetic configurations due to the adsorption of 3d TM adatoms: Mn ($\mu = 5\ \mu_\beta$), V ($\mu = 1\ \mu_\beta$), and Zn ($\mu = 0\ \mu_\beta$) respectively (from left to right). Blue and pink represent opposite magnetization states.

monolayer where the adsorbing carbon atoms move toward the foreign atom.

Because TM elements include the largest number of valence electrons and shortest atomic radii among studied metallic atoms, the ones that form the strongest bonds with the monolayer come from these elements including Ni, Ti, Co, Sc, Fe, and V with binding energies of −1.89, −1.84, −1.70, −1.69, −1.39, and −1.38 eV, respectively. In addition, the foreign atoms from group AM and group III make stronger interaction with C_3N compared with the ones from group AEM. The adsorption distance of metallic adatoms is larger than that of the other types as a consequence of their larger radii. Among the elements of the metallic type, Al and TM elements form shorter bonds to the surface due to their comparable small atomic radii.

Table 2 suggests that functionalization by all metallic species may not lead to metallic behavior of the monolayer. Among

DOI: 10.1021/acs.jpcc.7b04511
J. Phys. Chem. C 2017, 121, 18575−18583

metallic adatoms, Be, and Mg from AE metals and Cr, Ni, and Zn from 3d T metals cannot change the semiconducting nature of C_3N, and they involve energy gaps of 0.41, 0.40, 0.23, 0.49, and 0.38 eV, respectively. To further verify that functionalization can introduce conducting behavior to C_3N, we carried out HSE06 simulations for some systems including nonmetallic (H and P), semimetallic (B), and metallic (Li and Sc) adatoms. As shown in Figure 4, our hybrid functional calculations illustrate that the considered systems have the zero energy gap, which is in agreement with the PBE results.

The semiconducting and conducting behavior of functionalized monolayers suggest this 2D material as a potential candidate for many applications such as catalytic, solar cell, and electronic devices. Interestingly adsorption of Mn from the TM group induces the half-metallic properties composed of a conducting spin-up channel and an insulating spin-down channel with an electronic band gap of 0.43 eV, which makes this functionalized monolayer potentially valuable for the spintronic applications. Metallic adsorption on C_3N mainly results in the charge acceptance of the monolayer (see Figure 8), while, in the nonmetallic and semimetallic functionalization, the monolayer may both donate and accept charges. This nature of C_3N is consistent with the one from graphene, as listed in Tables 1 and 2.

Figures 9 and 10 illustrate the TDOS and PDOS profiles of C_3N interacting with metallic foreign atoms. While the functionalization of nonmetallic and metalloidic adatoms leads to p-type doping, the adsorption of many metallic ones from AM, EAM, and group III, such as Li, Na, K, Ca, and Al, mainly transfers the Fermi level to the conduction bond and causes n-type doping.

As can be seen in Figure 10, d-state electrons inducing magnetic properties play essential roles at the Fermi level during the adsorption of TM elements. Our magnetic moment calculations illustrate that the pristine C_3N and the monolayers interacting with nonmetallic, metalloidic, and metallic foreign atoms (except TM elements) present the nonmagnetic behavior, whereas the adsorption of most of the 3d TM elements results in a nonzero magnetic moment (see Figure 11). The exceptions occur when C_3N weakly interacts with Cr or when the monolayer is functionalized with Co, Ni, Cu, and Zn in which the 3d shell is almost filled, canceling out the total magnetization and rendering symmetric spin-up and spin-down electronic density profiles. It should be noted that by doubling the supercell size in the *x* and *y* directions, one can study the nature of transferred magnetic properties, that is, ferromagnetic and antiferromagnetic to the C_3N monolayer.[43]

4. CONCLUSIONS

We used first-principles PBE and HSE06 DFT calculations to investigate electronic -magnetic properties of a recently experimentally grown single layer 2D material (C_3N) functionalized by various adatoms. The calculations indicate that foreign adatoms prefer to be adsorbed on carbon sites of the monolayer. While the adsorption of metallic elements mostly occurs at H_{CC} and T_C sites, other atomic species would be attracted to B_{CC} and T_C ones. The C_3N surface accepts charge due to the adsorption of metallic adatoms, although it might both gain and lose charge in the interaction with non/semimetallic elements depending on the particle size, number of valence electrons, and electronegativity.

While bare C_3N behaves as a semiconductor, the functionalization with adatoms may alter this electronic character into the metallic or half-metallic one. Our DFT results suggest that many metallic elements introduce free electron (n-type doping) to C_3N, whereas nonmetallic and metalloidic species mostly create free holes (p-type doping). TM elements embedding d electronic states can induce magnetic properties to the monolayer.

Our calculations suggest that functionalized C_3N presents viable electromagnetic properties, which can be employed in a variety of applications, such as solar cells, photocatalysis, sensors, and electronic devices. This study highlights that the chemical functionalization of C_3N is a promising route toward tuning its properties, which can consequently motivate further experimental and theoretical studies. With respect to the future theoretical studies, the effect of various parameters on the adatom adsorption such as different DFT functionals and correction schemes and physical parameters such as adatom−adatom coupling/clustering and the magnetic/electric field effects is highly attractive to be explored.

■ ASSOCIATED CONTENT

Supporting Information

The Supporting Information is available free of charge on the ACS Publications website at DOI: 10.1021/acs.jpcc.7b04511.

Two tables listing the structural details of C_3N (lattice vectors and positions) and one figure illustrating the total energy as a function of vacuum space. (PDF)

■ AUTHOR INFORMATION

Corresponding Author

*E-mail: chandraveer.singh@utoronto.ca.

ORCID

Chandra Veer Singh: 0000-0002-6644-0178

Notes

The authors declare no competing financial interest.

■ ACKNOWLEDGMENTS

C.V.S. and M.M. gratefully acknowledge their financial support by University of Toronto, Connaught Global Challenge Award, and Hart Professorship. The computations were carried out through Compute Canada facilities, particularly SciNet and Calcul-Quebec. B.M. acknowledges support from European Research Council for COMBAT project (grant number 615132). We acknowledge their continued support.

■ REFERENCES

(1) Novoselov, K. S.; Geim, A. K.; Morozov, S. V.; Jiang, D.; Zhang, Y.; Dubonos, S. V.; Grigorieva, I. V.; Firsov, A. A. Electric Field Effect in Atomically Thin Carbon Films. *Science* **2004**, *306*, 666.

(2) Roldán, R.; Chirolli, L.; Prada, E.; Silva-Guillén, J. A.; San-Jose, P.; Guinea, F. Theory of 2D Crystals: Graphene and Beyond. **2017**, arXiv:1703.07200. arXiv.org e-Print archive https://arxiv.org/abs/1703.07200 (accessed May 29, 2017).

(3) Lee, C.; Wei, X.; Kysar, J. W.; Hone, J. Measurement of the Elastic Properties and Intrinsic Strength of Monolayer Graphene. *Science* **2008**, *321*, 385−8.

(4) Geim, A. K.; Novoselov, K. S. The Rise of Graphene. *Nat. Mater.* **2007**, *6*, 183−191.

(5) Geim, A. K.; Grigorieva, I. V. Van der Waals Heterostructures. *Nature* **2013**, *499*, 419−425.

(6) Mannix, A. J.; Kiraly, B.; Hersam, M. C.; Guisinger, N. P. Synthesis and Chemistry of Elemental 2D Materials. *Nature Reviews Chemistry* **2017**, *1*, 0014.

(7) Vogt, P.; De Padova, P.; Quaresima, C.; Avila, J.; Frantzeskakis, E.; Asensio, M. C.; Resta, A.; Ealet, B.; Le Lay, G. Silicene: Compelling

DOI: 10.1021/acs.jpcc.7b04511
J. Phys. Chem. C 2017, 121, 18575−18583

Experimental Evidence for Graphenelike Two-Dimensional Silicon. *Phys. Rev. Lett.* **2012**, *108*, 155501.
(8) Resta, A.; Leoni, T.; Barth, C.; Ranguis, A.; Becker, C.; Bruhn, T.; Vogt, P.; Le Lay, G. Atomic Structures of Silicene Layers Grown on Ag (111): Scanning Tunneling Microscopy and Noncontact Atomic Force Microscopy Observations. *Sci. Rep.* **2013**, *3*, 2399.
(9) Gao, J.; Zhang, G.; Zhang, Y. W. Exploring Ag (111) Substrate for Epitaxially Growing Monolayer Stanene: A First-Principles Study. *Sci. Rep.* **2016**, *6*, 29107.
(10) Xu, Y.; Yan, B.; Zhang, H. J.; Wang, J.; Xu, G.; Tang, P.; Duan, W.; Zhang, S. C. Large-Gap Quantum Spin Hall Insulators in Tin Films. *Phys. Rev. Lett.* **2013**, *111*, 136804.
(11) Scalise, E. Vibrational properties of silicene and germanene. In Vibrational Properties of Defective Oxides and 2D Nanolattices. *Springer International Publishing* **2014**, 61−93.
(12) Molle, A.; Goldberger, J.; Houssa, M.; Xu, Y.; Zhang, S. C.; Akinwande, D. Buckled Two-Dimensional Xene Sheets. *Nat. Mater.* **2017**, *16*, 163−169.
(13) Xiong, W.; Xia, C.; Wang, T.; Du, J.; Peng, Y.; Zhao, X.; Jia, Y. Tuning Electronic Structures of the Stanene Monolayer via Defects and Transition-Metal-Embedding: Spin-Orbit Coupling. *Phys. Chem. Chem. Phys.* **2016**, *18*, 28759−28766.
(14) Chintalapati, S.; Shen, L.; Xiong, Q.; Feng, Y. P. Magnetism in Phosphorene: Interplay between Vacancy and Strain. *Appl. Phys. Lett.* **2015**, *107*, 072401.
(15) Gao, D.; Shi, S.; Tao, K.; Xia, B.; Xue, D. Tunable Ferromagnetic Ordering in MoS_2 Nanosheets with Fluorine Adsorption. *Nanoscale* **2015**, *7*, 4211−4216.
(16) Ramasubramaniam, A.; Naveh, D. Mn-Doped Monolayer MoS_2: An Atomically Thin Dilute Magnetic Semiconductor. *Phys. Rev. B: Condens. Matter Mater. Phys.* **2013**, *87*, 195201.
(17) Ding, Y.; Wang, Y. Structural, Electronic, and Magnetic Properties of Adatom Adsorptions on Black and Blue Phosphorene: A First-Principles Study. *J. Phys. Chem. C* **2015**, *119*, 10610−10622.
(18) Naqvi, S. R.; Hussain, T.; Luo, W.; Ahuja, R. (2017). Exploring Doping Characteristics of Various Adatoms on Single-layer Stanene. *J. Phys. Chem. C* **2017**, *121*, 7667−7676.
(19) Chan, K. T.; Neaton, J. B.; Cohen, M. L. First-Principles Study of Metal Adatom Adsorption on Graphene. *Phys. Rev. B: Condens. Matter Mater. Phys.* **2008**, *77*, 235430.
(20) Sahin, H.; Peeters, F. M. Adsorption of Alkali, Alkaline-Earth, And 3D Transition Metal Atoms on Silicene. *Phys. Rev. B: Condens. Matter Mater. Phys.* **2013**, *87*, 085423.
(21) Pang, Q.; Li, L.; Zhang, L. L.; Zhang, C. L.; Song, Y. L. Functionalization of Germanene by Metal Atoms Adsorption: A First-Principles Study. *Can. J. Phys.* **2015**, *93*, 1310−1318.
(22) Kadioglu, Y.; Ersan, F.; Gokoglu, G.; Akturk, O. U.; Aktürk, E. Adsorption of Alkali and Alkaline-Earth Metal Atoms on Stanene: A First-Principles Study. *Mater. Chem. Phys.* **2016**, *180*, 326−331.
(23) Li, Y.; Xia, C.; Du, J.; Xiong, W.; Li, X.; Wei, S. Influences of the Adsorption of Different Elements on the Electronic Structures of a Tin Sulfide Monolayer. *Phys. Chem. Chem. Phys.* **2017**, *19*, 5423−5429.
(24) Lalitha, M.; Mahadevan, S. S.; Lakshmipathi, S. Improved Lithium Adsorption in Boron- and Nitrogen-Substituted Graphene Derivatives. *J. Mater. Sci.* **2017**, *52*, 815−831.
(25) Tromer, R. M.; da Luz, M. G.; Ferreira, M. S.; Pereira, L. F. C. Atomic Adsorption on Nitrogenated Holey Graphene. *J. Phys. Chem. C* **2017**, *121*, 3055−3061.
(26) Mahmood, J.; Lee, E. K.; Jung, M.; Shin, D.; Choi, H. J.; Seo, J. M.; Jung, S. M.; Kim, D.; Li, F.; Lah, M. S.; et al. Two-Dimensional Polyaniline (C_3N) from Carbonized Organic Single Crystals in Solid State. *Proc. Natl. Acad. Sci. U. S. A.* **2016**, *113*, 7414−7419.
(27) Blinova, N. V.; Stejskal, J.; Trchova, M.; Ciric-Marjanovic, G.; Sapurina, I. Polymerization of Aniline on Polyaniline Membranes. *J. Phys. Chem. B* **2007**, *111*, 2440−2448.
(28) Chang, M. Y.; Wu, C. S.; Chen, Y. F.; Hsieh, B. Z.; Huang, W. Y.; Ho, K. S.; Hsieh, T. H.; Han, Y. K. Polymer Solar Cells Incorporating One-Dimensional Polyaniline Nanotubes. *Org. Electron.* **2008**, *9*, 1136−1139.
(29) Alam, M. M.; Wang, J.; Guo, Y.; Lee, S. P.; Tseng, H. R. Electrolyte-Gated Transistors Based on Conducting Polymer Nanowire Junction Arrays. *J. Phys. Chem. B* **2005**, *109*, 12777−12784.
(30) Ciric-Marjanovic, G. Recent Advances in Polyaniline Research: Polymerization Mechanisms, Structural Aspects, Properties and Applications. *Synth. Met.* **2013**, *177*, 1−47.
(31) Xiang, H. J.; Huang, B.; Li, Z. Y.; Wei, S. H.; Yang, J. L.; Gong, X. G. Ordered Semiconducting Nitrogen-Graphene Alloys. *Phys. Rev. X* **2012**, *2*, 011003.
(32) Mortazavi, B. Ultra-High Stiffness and Thermal Conductivity of Graphene Like C_3N. *Carbon* **2017**, *118*, 25−34.
(33) Wang, H.; Wu, H.; Yang, J. C_3N: A Two Dimensional Semiconductor Material with High Stiffness, Superior Stability and Bending Poisson's Effect. **2017**, arXiv:1703.08754. arXiv.org e-Print archive. https://arxiv.org/abs/1703.08754 (accessed May 27, 2017).
(34) Kresse, G.; Furthmüller, J. Efficient Iterative Schemes for *Ab-Initio* Total-Energy Calculations Using a Plane-Wave Basis Set. *Phys. Rev. B: Condens. Matter Mater. Phys.* **1996**, *54*, 11169.
(35) Kresse, G.; Joubert, D. From Ultrasoft Pseudopotentials to the Projector Augmented-Wave Method. *Phys. Rev. B: Condens. Matter Mater. Phys.* **1999**, *59*, 1758.
(36) Perdew, J. P.; Burke, K.; Ernzerhof, M. Generalized Gradient Approximation Made Simple. *Phys. Rev. Lett.* **1996**, *77*, 3865.
(37) Grimme, S. Semiempirical GGA-Type Density Functional Constructed with a Long-Range Dispersion Correction. *J. Comput. Chem.* **2006**, *27*, 1787−1799.
(38) Vydrov, O. A.; Scuseria, G. E. Assessment of a Long-Range Corrected Hybrid Functional. *J. Chem. Phys.* **2006**, *125*, 234109.
(39) Monkhorst, H. J.; Pack, J. D. Special Points for Brillouin-Zone Integrations. *Phys. Rev. B* **1976**, *13*, 5188.
(40) Tang, W.; Sanville, E.; Henkelman, G. A Grid-Based Bader Analysis Algorithm without Lattice Bias. *J. Phys.: Condens. Matter* **2009**, *21*, 084204.
(41) Yang, S.; Li, W.; Ye, C.; Wang, G.; Tian, H.; Zhu, C.; He, P.; Ding, G.; Xie, X.; Liu, Y.; et al. C_3N-A 2D Crystalline, Hole-Free, Tunable-Narrow-Bandgap Semiconductor with Ferromagnetic Properties. *Adv. Mater. (Weinheim, Ger.)* **2017**, *29*, 1605625.
(42) Nakada, K.; Ishii, A. Migration of Adatom Adsorption on Graphene Using DFT Calculation. *Solid State Commun.* **2011**, *151*, 13−16.
(43) Zhang, S.; Li, Y.; Zhao, T.; Wang, Q. Robust Ferromagnetism in Monolayer Chromium Nitride. *Sci. Rep.* **2015**, *4*, 5241.

DOI: 10.1021/acs.jpcc.7b04511
J. Phys. Chem. C 2017, 121, 18575−18583